RSC Advances

ROYAL SOCIETY OF CHEMISTRY

www.rsc.org/advances

One-step electrodeposition fabrication of superhydrophobic surface on aluminum substrate with enhanced self-cleaning and anticorrosion properties

Binbin Zhang [a, b], Yantao Li [a, *], Baorong Hou [a, *]

[a] *Key Laboratory of Marine Environmental Corrosion and Bio-fouling, Institute of Oceanology, Chinese Academy of Sciences, Qingdao 266071, China*
[b] *University of Chinese Academy of Sciences, Beijing 100049, China*

Corresponding Authors and E-mails:
ytli@qdio.ac.cn (Prof. Li), brhou@qdio.ac.cn (Prof. Hou)

Abstract:

This paper presents a facile, low-cost, one-step approach to fabricate a superhydrophobic surface via electrodepositing aluminum in an ethanol solution containing cerium nitrate hexahydrate and myristic acid. The wettability, morphology and chemical composition of the as-prepared surfaces were characterized by water contact angle (WCA), scanning electron microscopy (SEM), energy dispersive spectrometer (EDS), and Fourier transform infrared spectroscopy (FTIR). The highest WCA of the as-prepared surface after one-step electrodeposition process reaches to 162.1 °. Water droplet adhesion force, water stream reflecting, water droplet bouncing, and self-cleaning properties were investigated respectively. Potentiodynamic polarization and electrochemical impedance spectroscopy (EIS) tests demonstrated that the as-prepared superhydrophobic surface greatly improved the corrosion resistance of the aluminum substrate. The corrosion current density (I_{corr}) of the as-prepared superhydrophobic surface is smaller by more than 3 orders of magnitude. The presented method is facile, low-cost, and relatively environmental friendly, which has a promising application in anticorrosion and anticontamination fields.

Key words: superhydrophobic, aluminum, one-step electrodeposition, self-cleaning, anticorrosion

1. Introduction

In nature, biological organisms smartly control their surface wettability on multiscale structures to help them control their interaction with water and survive in harsh environments [1-3]. These natural surfaces provide inspirations in designing and fabricating functional interfacial materials with unique wettability [4]. Inspired by the self-cleaning lotus leaf [5-6] and "anti-water" leg of a water strider [7], the use of artificial superhydrophobic surfaces with water contact angle lager than 150° and sliding angle smaller than 10° has been considered as one of the promising methods for its potential application in corrosion protection [8-14]. Superhydrophobic films have been proven to

inhibit the corrosion of metal in aqueous solutions result from the presence of air between superhydrophobic surface and corrosion medium [15-19].

Given the significant status in the application for the modern industry, aluminum and its alloys have attracted considerable interest and been widely used in the aerospace, machinery manufacturing and electronic industries for their excellent properties, such as high-specific strength, excellent heat conductivity, excellent electrical conductivity, and low-specific weight. Nevertheless, aluminum is a very active metal and easily corrodes in aqueous solutions or a humid atmosphere, which seriously prevents the large-scale application of aluminum and its alloys. Therefore, fabricating superhydrophobic surface on aluminum is of great significance, and considered as a promising approach to enhance the anticorrosion performance of aluminum and its alloys.

Up to now, a great number of methods have been successfully developed to fabricate artificial superhydrophobic surfaces, such as chemical etching [20-24], anodic oxidation [25-30], sol-gel processing [31-32], chemical vapor deposition [33], solution-immersion [34], colloidal template [35], laser fabrication [36], spin-coating [37], hydrothermal [38] etc. For example, Liao et al. [24] fabricated a superhydrophobic aluminum surface using a chemical etching method, and investigated the static/dynamic anti-icing behaviors of the as-prepared surface. Lu et al. [27] and Wang et al. [28] prepared superhydrophobic surfaces on aluminum substrate as a barrier to atmospheric and microbiological corrosion with anodisation method followed by fluorination treatment. Liu et al. [30] reported a method including anodic oxidation and self-assembly process for controllable fabrication of a robust superhydrophobic aluminum alloy surface, and the as-prepared surface shown good corrosion resistance, self-cleaning, mechanical and chemical stability. Wang et al. [38] fabricated a superhydrophobic surface on 2024 aluminum alloy substrate via a facile hydrothermal approach, and found that the superhydrophobic film considerably improved the corrosion resistance of the substrate. However, most of the methods mentioned above involve two steps, namely, the construction of micro/nanostructured roughness and low surface energy modification [39-49]. These methods usually require special conditions, expensive materials, time consuming and complex multistep operations, limiting their practical applications. Furthermore, many methods involve the use of biological poisonous materials, such as fluoroalkylsilane (FAS), to achieve a low surface energy. If both processes can be done in just one step, the process of preparing superhydrophobic surfaces would be simplified and the fabrication time would be shorted. Therefore, a general, inexpensive, and operationally convenient method is highly demanded, which would be very advantageous for large-scale industrial production.

Currently, electrodeposition has emerged as a competitive technique to fabricate superhydrophobic surfaces because of its advantages such as easy control, simplicity, low cost, and ability to make large-area surfaces. To the best of our knowledge, a rapid one-step electrodeposition method to create a corrosion-resistant superhydrophobic surface based on aluminum substrate or its alloys has relatively rare been studied and reported.

In this paper, a facile, low-cost one-step electrodeposition method was used to fabricate a superhydrophobic surface on aluminum substrate. The influences of the electrodeposition parameters (including electrodeposition voltage and electrodeposition time) were evaluated. The water adhesion force, water stream reflecting, water droplet bouncing, and self-cleaning properties were measured, demonstrating the excellent superhydrophobicity of the as-prepared surface. The electrochemical tests (including polarization and EIS) in 3.5 wt % NaCl aqueous solutions were used to investigate the anticorrosion performance of the surface. This method provides a facile, fast process to protect the surface of aluminum from corroding. Compared with other methods fabricating superhydrophobic surfaces, this approach has the advantages of simple operation, low cost, low toxicity, and convenience, and it may greatly expand the applications of aluminum and its alloys.

2. Experimental details

2.1. Materials and reagents

Aluminum (99.99 wt. %) foil was purchased from Beijing Goodwill Metal Technology Co., Ltd. Other reagents, including perchloric acid, ethanol, cerium (Ⅲ) nitrate hexahydrate, myristic acid (MA), and sodium chloride, were all purchased from Sinopharm Chemical Reagent Co., Ltd. and used as received. All of the reagents were of analytical grade. Moreover, deionized water with a resistivity of 18.2 MΩ•cm was used in all of the experiments.

2.2. Electropolishing

Aluminum foil (20 mm×20 mm×1 mm) was used in the one-step electrodeposition experiment without an annealing step. The specimens were ultrasonically cleaned with ethanol for 10 min followed by deionized water for another 10 min, and then dried with blower. Before electrodeposition, aluminum substrates were electrochemically polished in a 25 mL mixture of perchloric acid and ethanol ($HClO_4$:C_2H_5OH = 1:4 in volumetric ratio, 5 ℃). The electropolishing process was carried out with 20 V applied potential between aluminum and a counter electrode (platinum plate) for 4 min. The distance between the two electrodes is 2 cm. The electrolyte was vigorously stirred during the electropolishing process.

2.3. One-step electrodeposition process

Cerium (Ⅲ) nitrate hexahydrate (0.05 M) and myristic acid (0.2 M) immersed in ethanol was used as the electrodeposition electrolyte. The elecrodeposition process was performed on a direct-current power supply at a constant voltage for a certain time at room temperature, where the specimen was used as the cathode and the platinum plate as the anode. The cathodic specimen and the anodic platinum plate were separated by a distance of 2 cm. After deposition, the specimen was removed from the electrolyte, immediately rinsed thoroughly with ethanol, and dried under atmospheric conditions.

2.4. Characterization and Tests

The water contact angle (WCA) of the surface was measured with a contact-angle meter (JC2000C1, Shanghai Zhongchen Digital Technic Apparatus Co., Ltd.) with 4ul drops of distilled water at room temperature. The average value was determined by

measuring the same sample at five different positions. The morphology of the as-prepared superhydrophobic surface was characterized with scanning electron microscopy (SEM, S-3400N) equipped with an EDS at 20 kV. The chemical composition was analyzed by Fourier transform infrared spectroscopy (FTIR, Nicolet iSIO spectrometer). Water droplet adhesion force was judged by the sliding process of water droplet on the as-prepared superhydrophobic surface. Water flow reflecting and water droplet bouncing were carried out using an injection needle (1 mL, ignoring the influence of the air resistance).

The corrosion resistance of the aluminium sample was investigated by electrochemical impedance spectroscopy (EIS) and potentiodynamic polarization curves, which were performed in 3.5 wt.% NaCl aqueous solution at room temperature. All electrochemical experiments were conducted using Gamry Reference 3000 (USA). The electrochemical experiments were carried out in a conventional three-electrode cell configuration with platinum as the counter electrode, Ag/AgCl (3 M KCl) as the reference electrode and the aluminum samples as the working electrode. EIS was carried out at open circuit potential (OCP) in the frequency range of 10 mHz-100 kHz with AC signals of amplitude 10 mV peak to peak. The polarization curves were obtained at a scan rate of 1 mV/s and started from a potential of -250 mV to +250 mV vs. OCP after 8 cycles. Before the tests, the specimens were immersed in the test solution for about 30 min to stabilize, until the primarily corrosion potential reached a steady state. Each result was repeated for at least 5 times. All measurements were performed at 298 K.

3. Results and discussion

3.1. Schematic illustration of the fabrication of superhydrophobic surface

Figure 1 shows the fabrication process of the superhydrophobic surface on Al substrate. Al foil was firstly electropolished before deposition process. Then, the one-step electrodeposition fabrication was carried out in an ethanol solution containing cerium nitrate hexahydrate and myristic acid. When the DC voltage is applied to the electrodes, the Ce^{3+} ions near the cathode react with MA to form cerium myristate and hydrogen ions (H^+). Meanwhile, the concentration of free H+ ions in the solutions increases, and some of them gain electrons to form H_2. The reaction equations are described as follows:

$$Ce^{3+} + 3CH_3(CH_2)_{12}COOH \rightarrow Ce(CH_3(CH_2)_{12}COO)_3 + 3H^+ \quad (1)$$

$$3H^+ + 3e^- \rightarrow 3/2H_2 \quad (2)$$

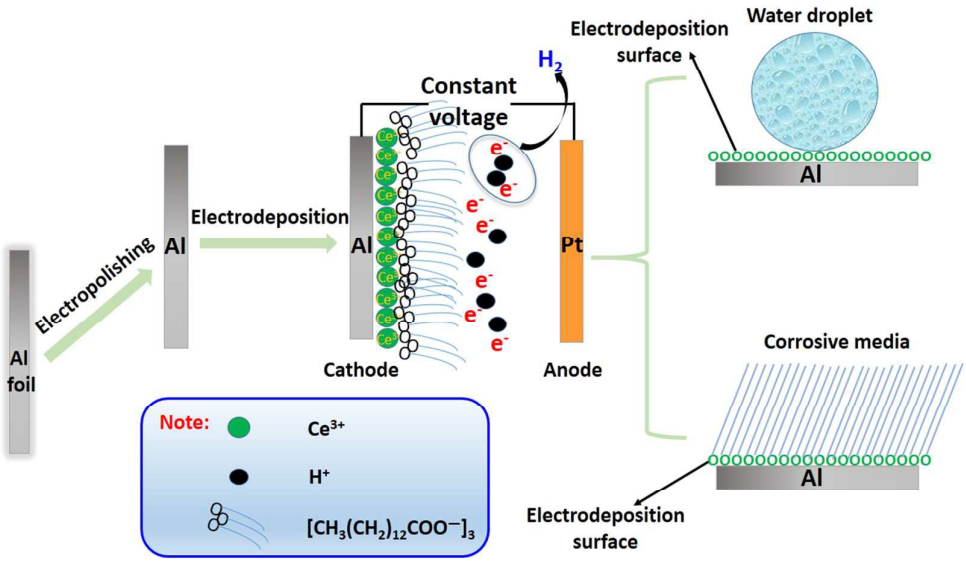

Figure 1. Schematic diagram of the fabrication of superhydrophobic surface on Al substrate.

After the electrodeposition process, superhydrophobic surface was obtained. The hydrophobicity, adhesion force, self-cleaning, and anticorrosion performance were evaluated in order.

3.2. Effect of electrodeposition voltage on morphology and wettability

Figure 2 shows SEM images of the as-prepared surface under different electrodeposition voltages for 3 h. Figure 2(a) shows the SEM morphology of the specimen at an electrodeposition voltage of 10 V, in which the papilla structure was visible formed. Figure 2(b) shows an SEM images of the specimen at a voltage of 20 V, in which the papilla structure has begun to agglomerate as papillae particles distributed randomly on the surface, and hierarchical micro/nanopapillae structures were constructed. As shown in Figure 2(c) and (d), when the voltage was increased to 30 V and 40 V respectively, the agglomerated papilla particles were gathered to form larger papilla particles, the hierarchical papillae structures were gradually unsharp, but they were relatively distributed homogeneous. As shown in Figure 2(e) and (f), the voltage was 50 V and 60 V respectively, the papillae gathered into a mushroom head structures, which have larger size. They were not distributed as homogeneously as shown in Figure 2(b), which may be attributed to discharge and partial damage to the structure under such a high voltage.

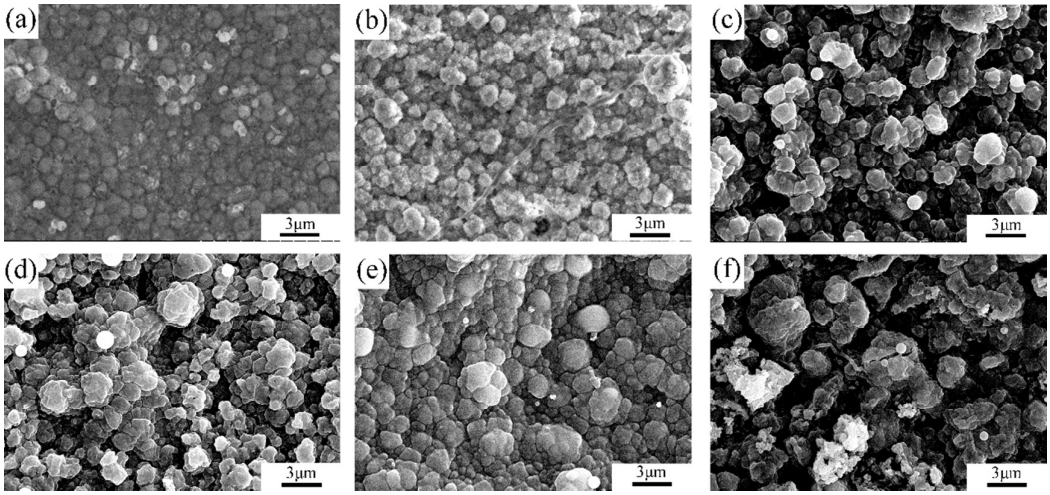

Figure 2. SEM images of the as-prepared superhydrophobic surfaces obtained at different electrodeposition voltages: (a) 10 V, (b) 20 V, (c) 30 V, (d) 40 V, (e) 50 V, and (f) 60 V.

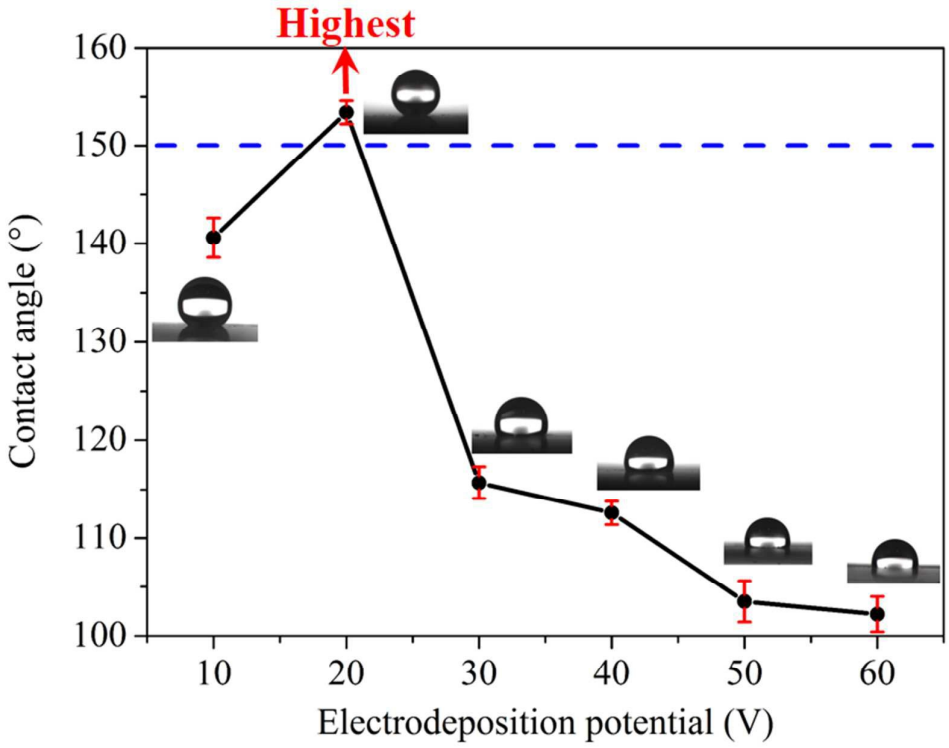

Figure 3. Variation in the water contact angles of the surfaces as functions of the electrodeposition voltage.

As illustrated in Figure 2, the morphology of the surface varied with the electrodeposition voltage. The corresponding static water contact angles were measured, and the results are shown in Figure 3. The contact angle reached 140.6 ° at a deposition voltage of 10 V. When the deposition voltage was increased to 20 V, the largest contact angle of 153.4 ° was obtained. When the deposition voltage became 30 V, the contact angle was decreased sharply to 115.7 °. When the electrodeposition

voltage was further increased to 40 V, the contact angle was 112.6 °, which is similar with the CA of 30 V. Moreover, when the electrodeposition was continuously increased to 50 V and 60 V, the contact angles became 103.5 ° and 102.2 °, respectively. The increasing of the electrodeposition voltage induced the agglomeration of the papillaes, which made the size of the particles become bigger and bigger. The air layer entrapped between papillaes was mainly influenced by the surface morphology. With the increasing of the voltage, the air entrapment was less and less, which result in the decrease of the hydrophobicity. According to the results above, the as-prepared surface at a voltage of 20 V exhibits best superhydrophobicity. As known to us, the wettability was controlled by the surface structure and chemical composition. The hierarchical micro/nanoscaled papillae structure has a better ability to trap air and increase the superhydrophobicity of the surface.

3.3. Effect of electrodeposition time on morphology and wettability

In order to study the effect of the electrodeposition processing time on the wettability, SEM images of the as-prepared surfaces with different electrodeposition times at an electrodeposition voltage of 20 V were obtained in Figure 4. After electrodeposition for 1 min (Figure 4a), many small papillae particles were heterogeneously distributed on the surface. When the elctrodeposition time was extended to 5 min (Figure 4b), the small papillae began to connect with each other and agglomerate as larger papillae. When electrodeposition time was prolonged to 10, 20, 30, 60, 90, 120, 150, and 180 min (Figure 4c, d, e, f, g, h, i, and j), the agglomeration process continued, and obviously homogeneous hierarchical papillae structure were constructed on the surface. However, when the process time was increased to 210 and 240 min (Figure 4k, l), the papillae monomer structure began to aggregate with each other, the particle size became larger. What's more, obviously small holes were generated as a result of discharge under the long-time current on the surface.

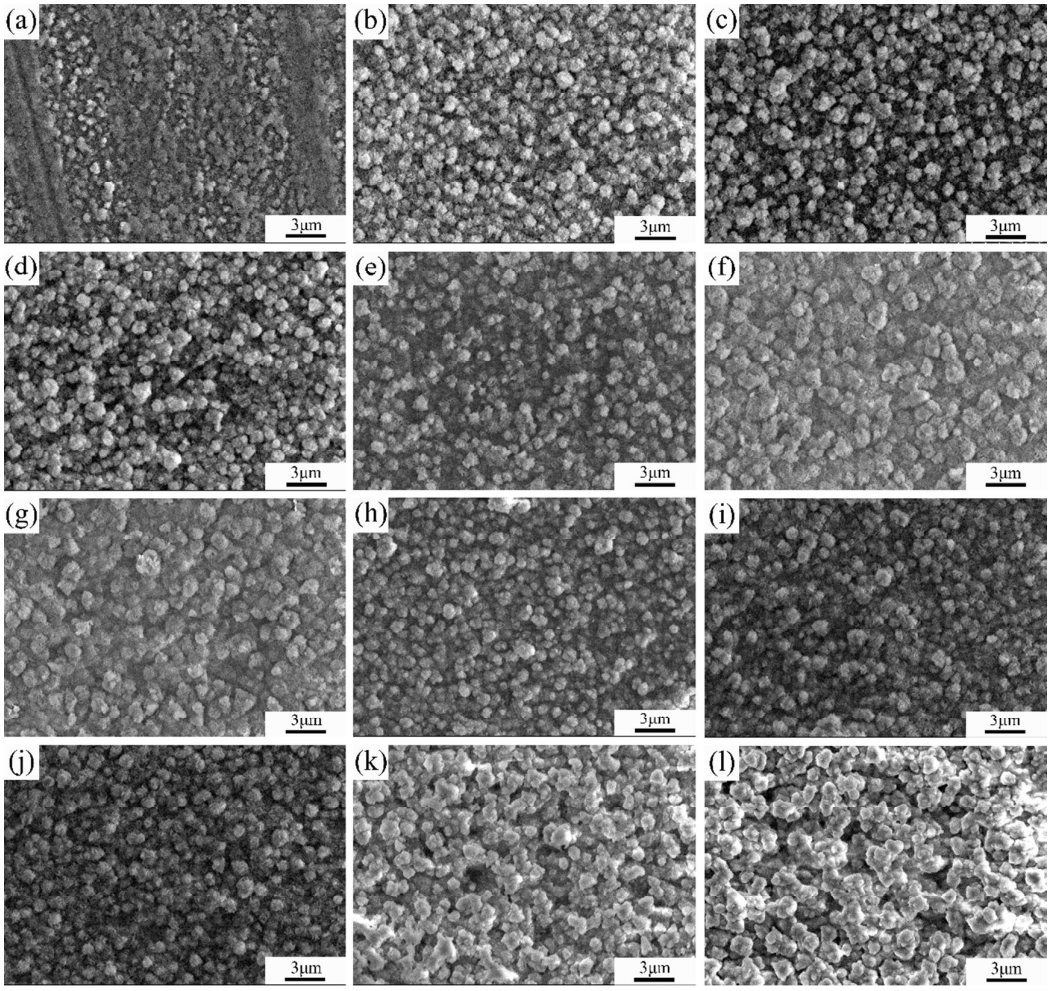

Figure 4. SEM images of the as-prepared superhydrophobic surfaces obtained at 20 V with different electrodeposition time: (a) 1 min, (b) 5 min, (c) 10 min, (d) 20 min, (e) 30 min, (f) 60 min, (g) 90 min, (h) 120 min, (i) 150 min, (j) 180 min, (k) 210 min, and (l) 240 min.

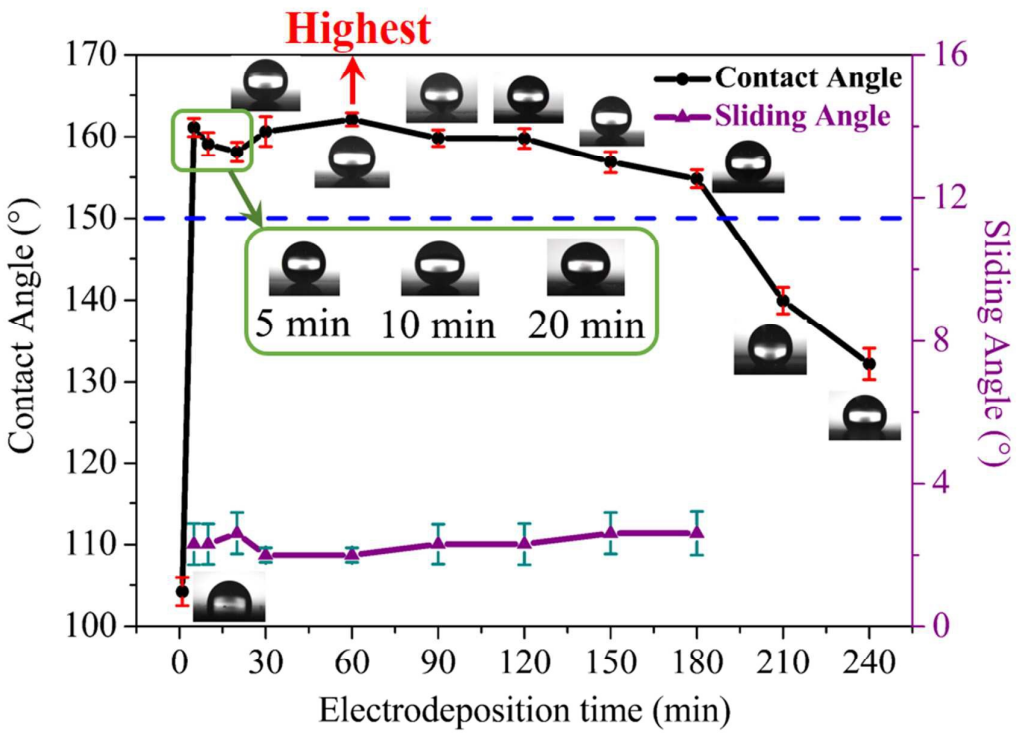

Figure 5. Variation in the water contact angles and sliding angles of the surfaces obtained at different electrodeposition time at a voltage of 20 V.

The corresponding contact angles and sliding angles are plotted versus electrodeposition time in Figure 5. After the electrodeposition of 1 min, the water contact angle of the as-prepared surface was 104.2 °. When the electrodeposition time prolonged to 5, 10, 20, 30, 60, 90, 120, 150, and 180 min, the contact angles were all above 154 °, and the sliding angles were all less than 3 °, which indicates that the as-prepared surfaces exhibit excellent superhydrophobicity. When the electrodeposition time was 210 and 240 min, the contact angles decreased to 139.9 ° and 132.2 °, respectively. The sliding angles were not available when the electrodeposition time was 1 min, 210 min and 240 min, meaning the droplet was stuck even when it turned upside down. According to the contact angles and sliding angles above, it can be concluded that the surface exhibited excellent superhydrophobicity (Contact Angle=162.1°, SA~2.0±0.5 °) under a voltage of 20 V when the electrodeposition time was longer than 5 min, and shorter than 180-190 min.

3.4. Characteristics and chemical composition of the superhydrophobic surface

On the basis of the analysis of the effect of electrodeposition voltage and electrodeposition time on the morphology and wettability, an electrodeposition voltage of 20 V and electrodeposition time of 60 min were chosen as the optimal parameters to fabricate the superhydrophobic surface.

SEM images and water contact angle under optimal parameters were shown in Figure 6. Papillae structures were obtained and distributed homogeneously under optimal parameters. Under higher magnification, nano structures can be seen on the micro papillae structures. After the hierarchical micro/ nanopapillae structures were

obtained, the CA increased to 162.1 ° compared with 45.9 ° for the substrate after electropolishing, indicating that the specimen exhibited excellent water repellency and a superhydrophobic surface was acquired.

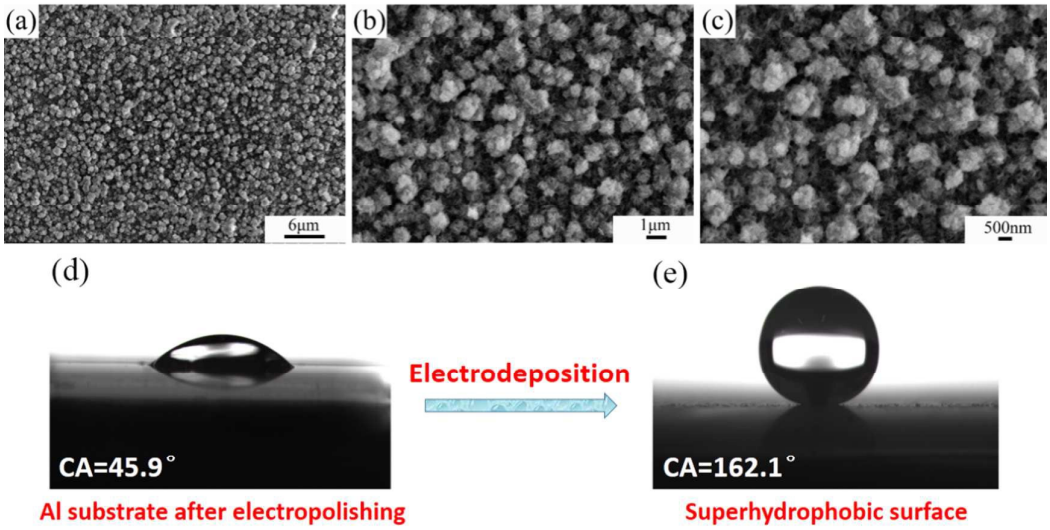

Figure 6. SEM images under different magnifications and contact angles. (a) ×2500, (b) ×7500, (c) ×10000, (d) CA after electropolishing process, and (e) CA after electrodeposition process**.**

It is well-know that hierarchical micro/nanoscaled papillae structures plays an important role in the wettability of a solid surface. A large amount of air can be trapped in the gaps generated in the hierarchical structure, which can lead to the larger CA and smaller SA according to the Cassie-Baxter equation: [50-51]

$$\cos\theta_r = f_1 \cos\theta - f_2 \quad (3)$$

$$f_1 + f_2 = 1 \quad (4)$$

where f_1 is the area fraction of the water-solid interface; f_2 is the area fraction of the water-air interface; θ_r represent the water contact angle of the micro/nanostructured surface; and θ is that of the smooth surface.

Given in the above illustration, the maximum contact angle on the superhydrophobic surface is 162.1 °, while that of the smooth plat surface with myristic acid is only about 109 ° [52]. When these angles are introduced into the above equation, it was calculated that f_1 is 0.071, demonstrating that the contact area fraction of the water-air interface is 0.929. The large contact area between the water and air is effective in preventing the penetration of water droplets into the surface. It is responsible for the excellent superhydrophobic property.

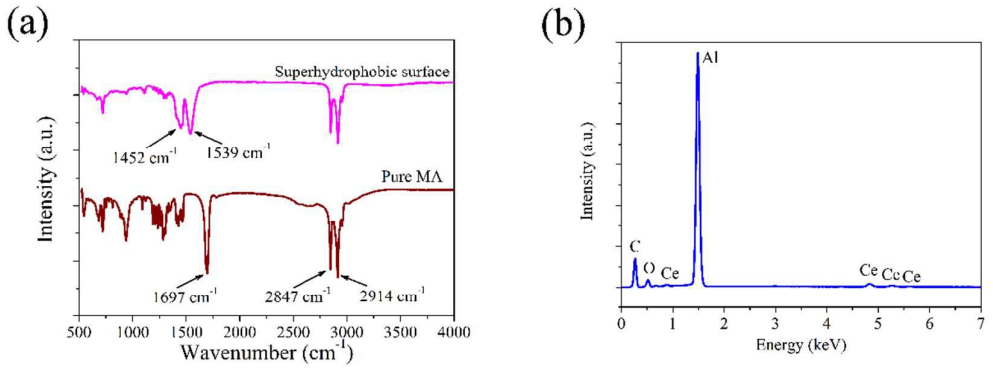

Figure 7. Chemical composition analysis of the superhydrophobic surface: (a) FTIR and (b) EDS

EDS and FTIR were utilized to analyze the chemical composition of the superhydrophobic surface. Figure 7 (a) reveals the FTIR spectra of pure MA and the superhydrophobic surface. In the high-frequency region of the two curves, the adsorption peaks at about 2847 and 2914 cm^{-1} are attributed to C-H asymmetric and symmetric stretching vibrations, respectively. In the low-frequency region, the peak for the carboxyl (-COO) group of MA at 1697 cm^{-1} is no longer present at the superhydrophobic surface. Two new peaks appear at 1539 and 1452 cm^{-1} that correspond to the appearance of carboxylate (cerium myristate). Figure 7 (b) shows the EDS regional analysis of the superhydrophobic sample. The presence of C, O, and Ce on the as-prepared surface can be observed in Figure 7 (b). On the basis of the chemical valences of Ce^{3+} and $CH_3(CH_2)_{12}COO^-$ in the solution, we can deduce that cerium myristate, $Ce(CH_3(CH_2)_{12}COO)_3$, is formed on the superhydrophobic surface. Consequently, the as-prepared superhydrophobic surface formed on the aluminum with low surface energy is cerium myristate.

3.5. Water droplet adhesion force, water stream reflecting, water droplet bouncing and self-cleaning properties

Given the superhydrophobicity of the as-prepared surface, the water droplet was hardly able to stick to the as-prepared surface and the sliding angle was extremely low (about 2 °), allowing water droplets to roll off quite easily. This can be demonstrated by evolving the sliding process of a water droplet on the as-prepared surface. The series of photographs (a)-(f) in Figure 8 showed the sliding process of a water droplet (~ 4 μL) on the as-prepared superhydrophobic surface. It can be seen that the surface was so hydrophobic that the water droplet is difficult to attach on the surface with the slightly increasing of the sliding angle, indicating an extremely low adhesion force between water droplet and as-prepared superhydrophobic surface during the rolling process.

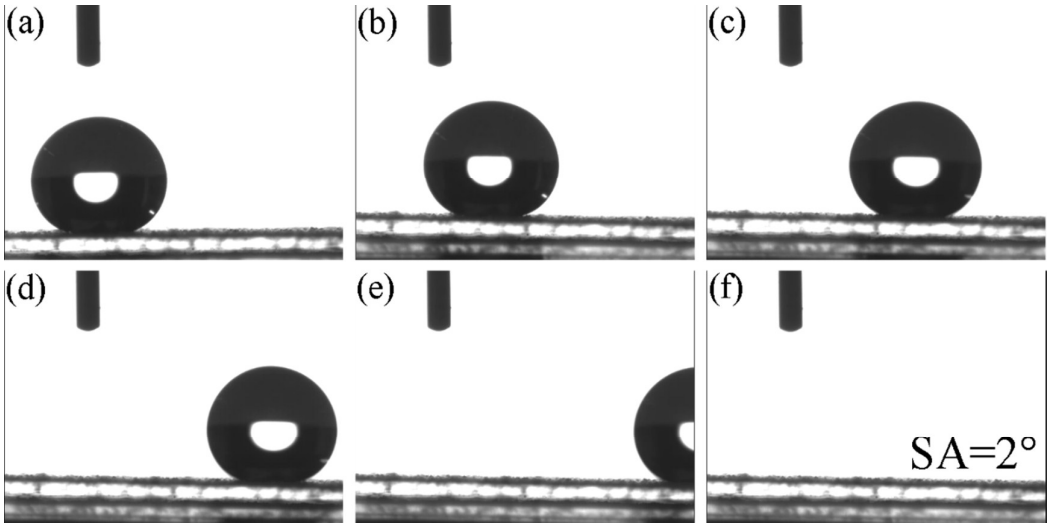

Figure 8. The images of the sliding process of a water droplet (~ 4 μL) on the as-prepared superhydrophobic surface.

The snapshots of water stream reflecting and water droplet bouncing of the as-prepared surface were shown in Figure 9 (a) and (b). Given the excellent superhydrophobicity of the surface, the surface could not be wetted and resist the attack of the water stream when water jet shoots water stream (speed, V ~ 0.5 m/s) toward the surface (Shooting angle, $\alpha = 40 \pm 0.5$ °). It is shown in Figure 9 (b) that the reflected water stream can still bounce off from the surface like a light reflection (Reflecting angle, $\beta = 20 \pm 0.5$ °) without leaving a trace, which further confirms the mentioned stability of as-prepared superhydrophobicity.

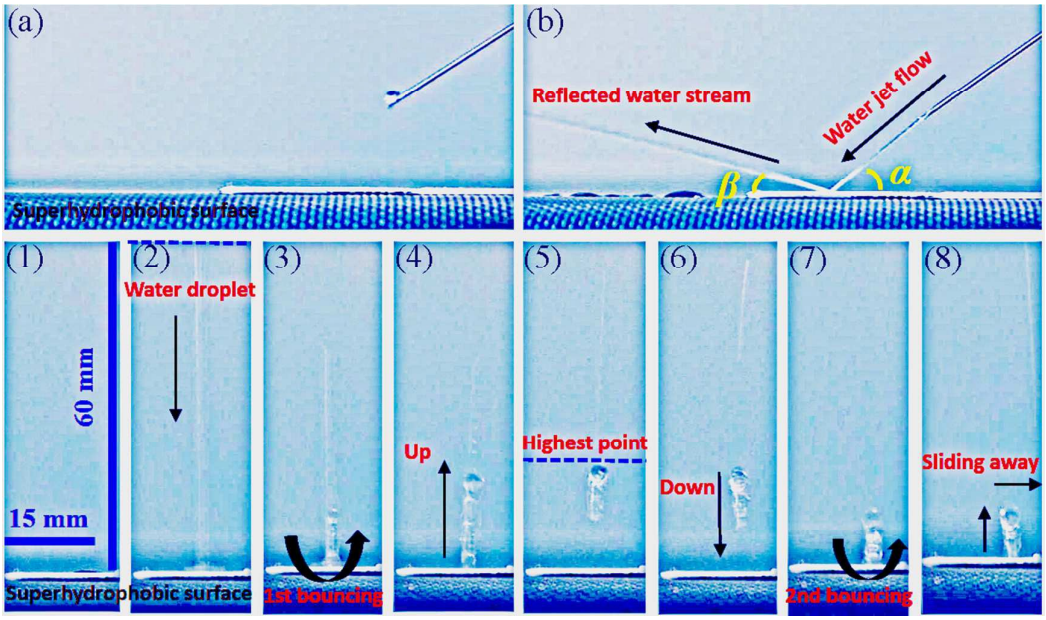

Figure 9. Snapshots of water stream reflecting and water droplet bouncing of the superhydrophobic surface, (a) the water jet is ready to shoot toward the surface, (b) the shooting and reflecting of the water stream, (1) a water droplet is ready to fall on the surface, (2) the water droplet reaches on the surface, (3) 1st bouncing of the water

droplet, (4) bouncing up of the water droplet, (5) the water droplet reaches to the highest point, (6) falling down of the water droplet, (7) 2nd bouncing of the water droplet, (8) water droplet bouncing up again and falls on the surface and slides away from left to right rapidly. The arrows represent the moving direction of the water droplet (Droplet size, ~ 5.7 ± 0.2 μL).

In addition, on a surface that shows water repellence, water droplets also tend to bounce and leave the surface instead of wetting or even contaminating the surface [53-57]. In other word, when water droplet happens to drop down from a very short distance, it can bounce up like an elastic ball. The water dropping and bouncing test of the as-prepared surface was shown in Figure 9 (1-8). The process was as follows: water dropping (Impacting speed, V ~ 1.1 m/s), 1st bouncing, bounce up, reaches to the highest point, droplet falling down again, 2nd bouncing, boucing up and then sliding away from the visual field. These water stream reflecting and water droplet bouncing investigations suggest that the sliding angle of the as-prepared surface is extremely low and that there is a very low resistance during the rolling process. What's more, the results show excellent superhydrophobicity and low adhesion force between water droplet and the surface again.

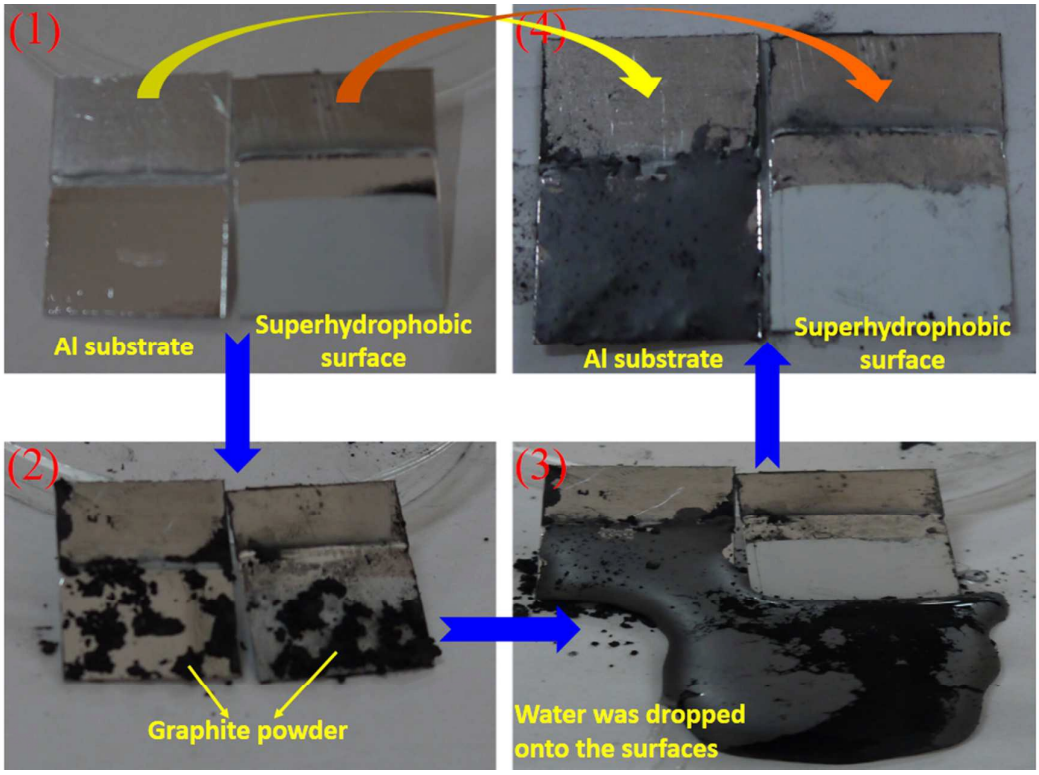

Figure 10. Self-cleaning test: (1) photo of Al substrate and superhydrophobic film-coated specimen before test, (2) photo of Al substrate and superhydrophobic film-coated specimen with graphite powder sprinkled on the surface, (3) photo of the same specimen after several water droplets were applied over the surface, (4) comparison of the specimen surface after self-cleaning test.

Self-cleaning test was also carried out using graphite powder. The Al substrate and superhydrophobic surface were fully contaminated by dirt (graphite powder). And

then, water was dropped onto the surfaces. The process and results of self-cleaning was shown in Figure 10. As shown in this Figure, much of the graphite powder was still spread and wetted by water droplets on the Al substrate surface after water dropping operation, while the superhydrophobic film-coated surface was much cleaner. Almost all the graphite powder was cleaned after the test, exhibiting excellent anti-adhesion and anti-contamination property of the as-prepared superhydrophobic surface.

3.6. Anticorrosion performance

Potentiodynamic polarization is widely used to evaluate the instantaneous corrosion rate of a tested specimen. The corrosion potential (E_{corr}) and corrosion current density (I_{corr}) parameters obtained from polarization curves directly reflect the electrochemical corrosion behavior. Generally, better corrosion resistance possesses a lower corrosion rate, which corresponds to a lower I_{corr} or a higher E_{corr}. Figure 11 (a) shows the potentiodynamic polarization curves for the aluminum substrate and the as-prepared superhydrophobic surface in NaCl corrosion media. It can be seen that the E_{corr} of the superhydrophobic surface in 3.5 wt % NaCl solution positively increased to –1.219±0.02 V from –1.301±0.02 V for the substrate. Accordingly, the I_{corr} in 3.5 wt % NaCl solution for the substrate is 7.16×10^{-8} A/cm^2, while after superhydrophobic treatment, the I_{corr} is 8.76×10^{-11} A/cm^2. Compared with the value for the substrate, the I_{corr} of the superhydrophobic surface is smaller by more than 3 orders of magnitude. The increase in E_{corr} and greatly decrease in I_{corr} suggest that the superhydrophobic surface greatly improved the corrosion resistance of the aluminum in NaCl solution. The potentiodynamic polarization results indicate that the superhydrophobic surface has an excellent corrosion resistance in NaCl aqueous corrosive media.

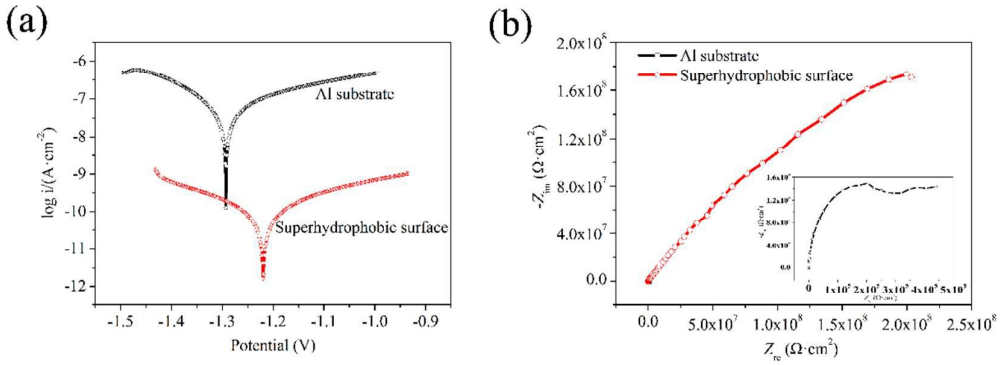

Figure 11. (a) Potentiodynamic polarization and (b) EIS curves of the bare and superhydrophobic surfaces in 3.5 wt % NaCl aqueous solutions.

Electrochemical impedance spectroscopy is often used as a supplement to potentiodynamic polarization for a better evaluation of the corrosion behavior. Figure 11 (b) displays the Nyquist plots of the bare aluminum and the as-prepared superhydrophobic surfaces. Many researchers have found that the capacitive loop at higher frequency is ascribed to the charge transfer resistance (R_{ct}) and that the diameter of the capacitive loop related to R_{ct} in the Nyquist plots represents the impedance of the samples. It can be clearly seen in Figure 11 (b) that the

superhydrophobic surface exhibited much higher impedance values in the 3.5 wt % aqueous solution of NaCl, indicating that the as-prepared superhydrophobic surface has a much better corrosion resistance in the above corrosion media.

Generally, when the aluminum substrate is immersed in the corrosion medium, the corrosion ions and water can easily contact the substrate and react with it. However, when the as-prepared superhydrophobic surface is immersed in the corrosion medium, the hierarchical structures are filled with air, which can effectively restrain the contact of the corrosion solution with the substrate. Therefore, the corrosion rate of the superhydrophobic specimen was much lower than that of the substrate in the corrosion solution medium.

4. Conclusion

In summary, a simple operation, low-cost, low toxicity, and one-step method was used to fabricate a superhydrophobic surface on an aluminum substrate by a facile electrodeposition process in an ethanol solution containing cerium nitrate hexahydrate and myristic acid. 20 V, 60 min was the optimal parameters of the electrodeposition process. The obtained surface is composed of cerium myristate with a hierarchical micro/nanoscale-particle structure and has a maximum contact angle of 162.1 °. Low adhesion force between water droplet and surface, excellent self-cleaning properties were achieved. The superhydrophobic surface shows excellent anticorrosion performance in 3.5 wt % NaCl aqueous solution. Compared with the value for the substrate, the I_{corr} of the superhydrophobic surface is smaller by more than 3 orders of magnitude. The cooperation of rough hierarchical structure and hydrophobic tail of $CH_3(CH_2)_{12}COO–$ plays a vital role in the formation of superhydrophobicity and enhanced corrosion resistance. This process can be extended to other long-chain fatty acids for their similar hydrophobic tails with low surface energy. This method provides a new thought to protect the surface of aluminum from corroding among hostile environment and may greatly expand the applications of aluminum and its alloys.

Acknowledgments

Financial supports from the National Natural Science Foundation of China (Grant No. 41276074) and Basic Research Project of Science & Technology Plan of Qingdao (Grant No. 13-1-4-122-jch) are gratefully acknowledged.

References

1. H. Bai, L. Wang, J. Ju, R. Sun, Y. Zheng and L. Jiang, Efficient water collection on integrative bioinspired surfaces with star-shaped wettability patterns, *Adv. Mater.*, 2014, 26, 5025-5030.
2. H. Bai, X. Tian, Y. Zheng, J. Ju, Y. Zhao and L. Jiang, Direction controlled driving of tiny water drops on bioinspired artificial spiders silks, *Adv. Mater.*, 2010, 22, 5521-5525.
3. Y. Zheng, H. Bai, Z. Huang, X. Tian, F. Q. Nie, Y. Zhao, J. Zhai and L. Jiang, Directional water collection on wetted spider silk, *Nature*, 2010, 463, 640-643.

4. H. Bai, J. Ju, Y. Zheng and L. Jiang, Functional fibers with unique wettability inspired by spider silks, *Adv. Mater.*, 2012, 24, 2786-2791.
5. L. Feng, S. Li, Y. Li, H. Li, L. Zhang, J. Zhai, Y. Song, B. Liu, L. Jiang and D. Zhu, Superhydrophobic surfaces, from natural to artificial, *Adv. Mater.*, 2002, 14, 1857–1860.
6. H. Wang, Z. Yang, J. Yu, Y. Wu, W. Shao, T. Jiang and X. Xu, Preparation of lotus-like hierarchical microstructures on zinc substrate and study of its wettability, *RSC Adv.*, 2014, 4, 33730-33738.
7. X. F. Gao and L. Jiang, Biophysics: water-repellent legs of water striders, *Nature*, 2004, 432, 36-36.
8. T. Liu, Y. S. Yin, S. G. Chen, X. T. Chang and S. Cheng, Super-hydrophobic surfaces improve corrosion resistance of copper in seawater, *Electrochim. Acta*, 2007, 52, 3709–3713.
9. Y. S. Yin, T. Liu, S. G. Chen, T. Liu and S. Cheng, Structure stability and corrosion inhibition of super-hydrophobic film on aluminium in seawater, *Appl. Surf. Sci.*, 2008, 255, 2978–2984.
10. T. Ishizaki, J. Hieda, N. Saito, N. Saito and O. Takai, Corrosion resistance and chemical stability of super-hydrophobic film deposited on magnesium alloy AZ31 by microwave plasma-enhanced chemical vapor deposition, *Electrochim. Acta*, 2010, 55, 7094–7101.
11. K. S. Liu and L. Jiang, Metallic surfaces with special wettability, *Nanoscale*, 2011, 3, 825–838.
12. S. Nishimoto and B. Bhushan, Bioinspired self-cleaning surfaces with superhydrophobocity, superoleophobicity, and superhydrophilicity, *RSC Adv.*, 2013, 3, 671-690.
13. X. Zhang, L. Wang and E. Levanen, Superhydrophobic surfaces for the reduction of bacterial adhesion, *RSC Adv.*, 2013, 3, 12003-12020.
14. B. N. Sahoo and B. Kandasubramanian, Recent progress in fabrication and characterization of hierarchical biomimetic superhydrophobic structures, *RSC Adv.*, 2014, 4, 22053-22093.
15. T. He, Y. C. Wang, Y. J. Zhang, Q. Iv, T. G. Xu and T. Liu, Super-hydrophobic surface treatment as corrosion protection for aluminium in seawater, *Corros. Sci.*, 2009, 51, 1757–1761.
16. P. Wang, D. Zhang and R. Qiu, Liquid/solid contact mode of super-hydrophobic film in aqueous solution and its effect on corrosion resistance, *Corros. Sci.*, 2012, 54, 77–84.
17. R. Qiu, D. Zhang and P. Wang, Superhydrophobic-carbon fibre growth on a zinc surface for corrosion inhibition, *Corros. Sci.*, 2013, 66, 350–359.
18. P. Wang, D. Zhang, R. Qiu, Y. Wan and J. Wu, Green approach to fabrication of a super-hydrophobic film on copper and the consequent corrosion resistance, *Corros. Sci.*, 2014, 80, 366–373.
19. Y. Liu, X. Yin, J. Zhang, S. Yu, Z. Han and L. Ren, A electro-deposition process for fabrication of biomimetic super-hydrophobic surface and its corrosion resistance on magnesium alloy, *Electrochim. Acta*, 2014, 125, 395–403.

20. X. W. Li, Q. X. Zhang, Z. Guo, J. G. Yu, M. K. Tang and X. J. Huang, Low-cost and large-scale fabrication of a superhydrophobic 5052 aluminum alloy surface with enhanced corrosion resistance, *RSC Adv.*, 2015, 5, 29639-29646.
21. N. Saleema, D. K. Sarkar, R. W. Paynter and X. G. Chen, Superhydrophobic aluminum alloy surfaces by a novel one-step process, *ACS Appl. Mater. & Interfaces*, 2010, 2, 2500-2502.
22. K. Nakayama, E. Tsuji, Y. Aoki and H. Habazaki, Fabrication of superhydrophobic hierarchical surfaces for low-surface-tension liquids, *RSC Adv.*, 2014, 4, 30927-30933.
23. X. Zhang, P. Y. Zhang, Z. Wu and Z. Zhang, Facile fabrication of stable superhydrophobic films on aluminum substrates, *J Mater. Sci.*, 2012, 47, 2757-2762.
24. R. J. Liao, Z. P. Zuo, C. Guo, Y. Yuan and A. Y. Zhuang, Fabrication of superhydrophobic surface on aluminum by continuous chemical etching and its anti-icing property, *Appl. Surf. Sci.*, 2014, 317, 701-709.
25. W. C. Wu, X. L. Wang, D. A. Wang, M. Chen, F. Zhou, W. M. Liu and Q. J. Xue, Alumina nanowire forests via unconventional anodization and super-repellency plus low adhesion to diverse liquids, *Chem. Comm.*, 2009, 9, 1043-1045.
26. X. J. Liu, W. C. Wu, X. L. Wang, Z. Z. Luo, Y. M. Liang and F. Zhou, A replication strategy for complex micro/nanostructures with superhydrophobicity and superoleophobicity and high contrast adhesion, *Soft Matter.*, 2009, 5, 3097-3105.
27. Z. Lu, P. Wang and D. Zhang, Superhydrophobic film fabricated on aluminium surface as a barrier to atmospheric corrosion in a marine environment, *Corros. Sci.*, 2015, 91, 287-296.
28. P. Wang, Z. Lu and D. Zhang, Slippery liquid-infused porous surfaces fabricated on aluminum as a barrier to corrosion induced by sulfate reducing bacteria, *Corros. Sci.*, 2015, 93, 159-166.
29. H. Wang, D. Dai and X. D. Wu, Fabrication of superhydrophobic surfaces on aluminum. *Appl. Surf. Sci.*, 2008, 254, 5599-5601.
30. C. Liu, F. Su and J. Liang, Facile fabrication of a robust and corrosion resistance superhydrophobic aluminum alloy surface by a novel method, *RSC Adv.*, 2014, 4, 55556-55564.
31. P. Van der Wal and U. Steiner, Super-hydrophobic surfaces made from Teflon, *Soft Matter*, 2007, 3, 426-429.
32. N. D. Hegde and A. Venkateswara Rao, Physical properties of methyltrimethoxysilane based elastic silica aerogels prepared by the two-stage sol-gel process, *J Mater. Sci.*, 2007, 42, 6965-6971.
33. T. Ishizaki, J. Hieda, N. Saito, N. Saito and O. Takai, Corrosion resistance and chemical stability of super-hydrophobic film deposited on magnesium alloy AZ31 by microwave plasma-enhanced chemical vapor deposition, *Electrochim. Acta.*, 2010, 55, 7094-7101.
34. M. Qu, B. Zhang, S. Song, L. Chen, J. Zhang and X. Cao, Fabrication of superhydrophobic surfaces on engineering materials by a solution-immersion

process, *Adv. Funct. Mater.*, 2007, 17, 593-596.
35. R. B. Pernites, C. M. Santos, M. Maldonado, R. R. Ponnapati, D. F. Rodrigues and R. C. Advincula, Tunable protein and bacterial cell adsorption on colloidally template superhydrophobic polythiophene films, *Chem. Mater.*, 2011, 24, 870-880.
36. B. K. Nayak, P. O. Caffrey, C. R. Speck and M. C. Gupta, Superhydrophobic surfaces by replication of micro/nano-structures fabricated by ultrafast-laser-microtexturing, *Appl. Surf. Sci.*, 2013, 266, 27-32.
37. Y. Liu, J. Zhang, S. Li, Y. Wang, Z. Han and L. Ren, Fabrication of a superhydrophobic graphene surface with excellent mechanical abrasion and corrosion resistance on an aluminum alloy substrate, *RSC Adv.*, 2014, 4, 45389-45396.
38. Z. Wang, J. Gong, J. Ma and J. Xu, In situ growth of hierarchical boehmite on 2024 aluminum alloy surface as superhydrophobic materials, *RSC Adv.*, 2014, 4, 14708-14714.
39. S. Shibuichi, T. Yamamoto, T. Onda and K. Tsujii, Super water- and oil-repellent surfaces resulting from fractal structure, *J. Colloid Interf. Sci.*, 1998, 208, 287-294.
40. M. Miwa, A. Nakajima, A. Fujishima, K. Hashimoto and T. Watanabe, Effects of the surface roughness on sliding angles of water droplets on superhydrophobic surfaces, *Langmuir*, 2000, 16, 5754-5760.
41. J. Genzer and K. Efimenko, Creating long-lived superhydrophobic polymer surfaces through mechanically assembled monolayers, *Science*, 2000, 290, 2130-2133.
42. A. Nakajima, K. Hashimoto, T. Watanabe, K. Takai, G. Yamauchi and A. Fujishima, Transparent superhydrophobic thin films with self-cleaning properties, *Langmuir*, 2000, 16, 7044-7047.
43. D. Schondelmaier, S. Cramm, R. Klingeler, J. Morenzin, C. Zilkens and W. Eberhardt, Orientation and self-assembly of hydrophobic fluoroalkylsilanes, *Langmuir*, 2002, 18, 6242-6245.
44. M. Ma, R. M. Hill, J. L. Lowery, S. V. Fridrikh and G. C. Rutledge, Electrospun poly(styrene-block-dimethylsiloxane) block copolymer fibers exhibiting superhydrophobicity, *Langmuir*, 2005, 21, 5549-5554.
45. B. Bhushan and Y. Jung, Natural and biomimetic artificial surfaces for superhydrophobicity, self-cleaning, low adhesion, and drag reduction, *Prog. Mater. Sci.*, 2011, 56, 1–108.
46. Z. Guo, W. Liu and B. L. Su, Superhydrophobic surfaces: from natural to biomimetic to functional, *J. Colloid Interf. Sci.*, 2011, 353, 335–355.
47. P. Wang, D. Zhang, R. Qiu and J. Wu, Super-hydrophobic metal-complex film fabricated electrochemically on copper as a barrier to corrosive medium, *Corros. Sci.*, 2014, 83, 317–326.
48. L. Li, Y. Zhang, J. Lei, J. He, R. Lv, N. Li and F. Pan, A facile approach to fabricate superhydrophobic Zn surface and its effect on corrosion resistance, *Corros. Sci.*, 2014, 85, 174–182.
49. Y. Tian and L. Jiang, Wetting: Intrinsically robust hydrophobicity, *Nature Mater.*, 2013, 12, 291-292.

50. A. B. D. Cassie and S. Baxter, Wettability of porous surfaces, *Trans. Faraday Soc.*, 1944, 40, 546-551.
51. W. Liang, L. Zhu, W. Li and H. Liu, Facile fabrication of a flower-like CuO/$Cu(OH)_2$ nanorob film with tunable wetting transition and excellent stability, *RSC Adv.*, 2015, 5, 38100-38110.
52. Z. Chen, F. Li, L. Hao, A. Chen and Y. Kong, One-step electrodeposition process to fabricate cathodic superhydrophobic surface, *Appl. Surf. Sci.*, 2011, 258, 1395-1398.
53. D. Richard, C. Clanet and D. Quere, Surface phenomena contact time of a bouncing drop, *Nature*, 2002, 417, 811-811.
54. J. C. Bird, R. Dhiman, H. M. Kwon and K. K. Varanasi, Reducing the contact time of a bouncing drop, *Nature*, 2013, 503, 385-388.
55. Y. Liu, L. Moevius, X. Xu, T. Qian, J. M. Yeomans and Z. Wang, Pancake bouncing on superhydrophobic surfaces, *Nature Physics*, 2014, 10, 515-519.
56. Y. Lu, S. Sathasivam, J. Song, C. R. Crick, C. J. Carmalt and I. P. Parkin, Robust self-cleaning surfaces that function when exposed to either air or oil, *Science*, 2015, 347, 1132-1135.
57. T. M. Schutzius, S. Jung, T. Maitra, G. Graeber, M. Kohme and D. Poulikakos, Spontaneous droplet trampolining on rigid superhydrophobic surfaces, *Nature*, 2015, 527, 82-85.

Table of Content

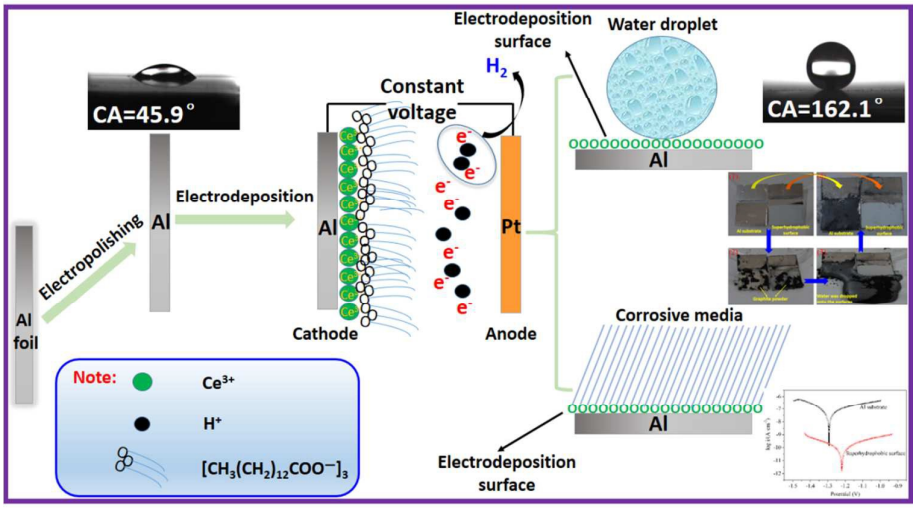

Superhydrophobic surface was successfully fabricated via a facile, low-cost one-step electrodeposition approach on aluminum substrate with excellent anticorrosion and self-cleaning properties.